Journal of Nuclear Materials 405 (2010) 33–43

Contents lists available at ScienceDirect

Journal of Nuclear Materials

journal homepage: www.elsevier.com/locate/jnucmat

Artificial neural network modeling for fission gas release in LWR UO_2 fuel under RIA conditions

Yang-Hyun Koo *, Jae-Yong Oh, Byung-Ho Lee, Young-Wook Tahk, Kun-Woo Song

Korea Atomic Energy Research Institute, 1045 Daedeok-daero, Yuseong, Daejeon 305-353, Republic of Korea

ARTICLE INFO

Article history:
Received 21 January 2010
Accepted 21 July 2010

ABSTRACT

A fission gas release (FGR) model was developed by using an artificial neural network method to predict fission gas release in UO_2 fuel under reactivity initiated accident (RIA) conditions. Based on the test data obtained in the CABRI test reactor and nuclear safety research reactor, the model takes into account the effect of the five parameters: pellet average burnup, peak fuel enthalpy, the ratio of peak fuel enthalpy to pulse width, fission gas release during base-irradiation, and grain size of a fuel pellet. The parametric study of the model, producing a physically reasonable trend of FGR for each parameter, shows that the pellet average burnup and the ratio of peak fuel enthalpy to pulse width are two of the most important parameters. Depending on the combination of input values for the five parameters, the application of the model to a fuel rod under typical RIA conditions of light water reactor produces 1.7–14.0% of FGR for the pellet average burnup ranging from 20 to 70 MW d/kg U.

1. Introduction

The behavior of light water reactor (LWR) UO_2 fuel under reactivity initiated accident (RIA) conditions is determined by many factors such as fission gas release (FGR), cladding state (oxidation and hydriding), pulse width, enthalpy increase, and so on. Fission gas release during RIA, which can be significantly enhanced by rapid temperature rise in fuel pellet, is important because it increases rod internal pressure, thereby contributing to the mechanical load on cladding. There is some experimental evidence that transient fission gas release resulting from adiabatic heating introduces a very rapid load increase that could lead to cladding rupture [1]. Therefore, modeling of fission gas release during an RIA event is required so that it can be used for analyzing fuel rod integrity under accident conditions and also for assessing radioactivity source term when fuel fails.

The gas release under RIA conditions depends on two factors; the initial conditions of fuel rod (fission gas inventory on grain boundaries associated with pellet average burnup and burnup distribution across pellet radial direction, width of high burnup structure (HBS) [2], and gap size just before RIA) and RIA test conditions (pulse width, fuel enthalpy increase, temperature distribution, and coolant temperature and pressure). According to the test results obtained in CABRI test reactor and nuclear safety research reactor (NSRR), it was found that there are some major parameters which dominantly affect gas release during an RIA event – fuel burnup, pulse width, and enthalpy increase. For example, it is generally agreed that, if other RIA test conditions are the same, fission gas release increases with burnup and fuel enthalpy [3]. However, it should be noted that other factors, which might be considered not so important, could also have a significant effect on gas release depending on the fuel and RIA conditions.

To understand the gas release data obtained from the RIA tests, several analytical models have been developed [4–7]. However, a mechanistic approach to correlate the measured gas release data with both fuel and accident conditions such as fuel burnup, HBS width, pulse width, and fuel enthalpy level has not been so successful partly because the number of gas release data points is small and the number of factors that should be considered is rather large. In this case, to perform more RIA tests that could reveal the effects of all relevant parameters would be the best approach for physics-based modeling. However, RIA test with irradiated fuel under typical LWR conditions is very difficult and costly as can be seen in the case of CABRI international program which is being carried out by the cooperation of many nations. And even if some more tests would be performed and consequently more data would be available than now, it would still be complex and difficult to develop a model that treats all the parameters mechanistically with a limited number of data.

Therefore, in this paper, an artificial neural network (ANN) [8] method is used to develop a model for predicting the fission gas release under RIA conditions. The ANN is a mathematical or a computational model based on biological neural networks. In more practical terms, neural networks are non-linear statistical data modeling tools that can be used to model complex relationships between inputs and outputs or to find patterns in data. One of the benefits of ANN model is that we can potentially better

* Corresponding author. Tel.: +82 42 868 8728; fax: +82 42 864 1089.
E-mail address: yhkoo@kaeri.re.kr (Y.-H. Koo).

0022-3115/$ - see front matter © 2010 Elsevier B.V. All rights reserved.
doi:10.1016/j.jnucmat.2010.07.032

understand the underlying physics via the consideration of small variations in both the input and out parameters.

2. FGR data under simulated RIA conditions

More than 80 RIA tests with pre-irradiated LWR fuel rods have been performed so far under simulated RIA conditions in pulse reactor experiments: special power excursion reactor (SPERT), power burst facility (PBF), CABRI reactor and NSRR [9]. In this work, only CABRI and NSRR data are analyzed because the RIA tests in the two reactors were performed for fuel rods whose burnup was moderate or high and hence gas release in these rods could affect fuel integrity significantly during RIA.

Test data for both the SPERT and PBF tests [10] were not considered in this work for two reasons. First, FGR data for the two tests were unavailable in the open literature. Second, even if FGR had been measured in the PBF test, FGR would probably have been very low due to fuel burnups that ranged from 0 to only 6 MW d/kg U, producing small FGR during RIA without applying a big additional load to cladding. Small FGR is expected here because fission gas inventory available for release during RIA – fission gas retained in the grain boundary – would have been low due to the limited time for the diffusion of fission gas atoms to the grain boundary to take place. A similar argument could be made for the SPERT-CDC test, where fuel burnups ranged from 1 to 13 MW d/kg U, except for two cases with burnup of 32 MW d/kg U. This is the basis on which the test data for both SPERT-CDC and PBF were omitted.

Table 1 shows only the data for fuel rods which kept integrity during the RIA simulating tests performed in the CABRI and NSRR [3,11–22]. In most cases, FGR data for failed fuel rods is not available for measurement because fission gas released to the pellet-cladding gap during both base-irradiation and/or RIA is leaked out through the failed cladding area during the RIA test. And even if fission gas release were measured for a few failed fuel rods, it is very likely that some amount of fission gas could have been leaked out of the test rods and therefore the measured gas would not represent the total gas that would have been actually released during the RIA test. Thus the FGR data for failed test fuel rods have been excluded.

There are two kinds of test data in Table 1. The first set of data is from the tests performed in the CABRI reactor, which consists of a driver core in a water pool and a test loop with liquid sodium as coolant [3]. While the loop was originally designed for research on liquid–metal-cooled reactors, it has been used extensively to test PWR fuel with a coolant temperature of 280 °C. Although heat transfer in sodium is better than that in water and hence this does not simulate exactly what happens in PWRs, this facility that can generate energetic pulse has been used to test high burnup fuel rods. In CABRI test, five data points that retained integrity during the RIA test are available for PWR UO_2 fuel [3,11].

The NSRR, where the RIA tests have been carried out in most cases with an experimental capsule filled with water at ambient temperature and ambient pressure [12], provides the second set of data. In these circumstances, fuel behavior including FGR would be different from what it would be under LWR operating conditions. Therefore, in a recent test of RH-2 [13], the coolant temperature of the test capsule was raised with an electric heater up to approximately 280 °C so that the test may simulate commercial reactor conditions.

Table 1 provides 29 data points for PWR fuel and the remaining 13 for BWR one (FK- and TS-series tests [14,15]). While hard gap closure occurs rather early in PWR fuel by cladding creepdown due to relatively thin cladding and high coolant pressure, BWR fuel with thick cladding in combination with low coolant pressure would produce much less gap closure by creepdown than PWR fuel for the same burnup. Consequently, under the same RIA test conditions, this could result in different temperature and stress distribution in the fuel pellets in BWR and PWR, producing different fuel behavior including fission gas release.

Grain size of the test fuel rods was provided for the only six tests. For the remaining 36 cases, grain sizes are assumed to be the same as that for typical LWR UO_2 fuel, 10 μm. As for the FGR during base-irradiation, it is assumed to be zero when this value is not available, and the justification for this assumption is given in Section 4.4.

3. Main parameters for RIA FGR

Of the many parameters that affects RIA FGR, five ones—pellet average burnup, peak fuel enthalpy, ratio of peak fuel enthalpy to pulse width, FGR during base-irradiation, and grain size of fuel pellet—are considered in this work. While the first three parameters are chosen because they are well known to affect RIA FGR significantly, the other two, FGR during base-irradiation and grain size, are selected because they can represent the degree of gas release path available during a RIA event.

In most cases, only fission gas accumulated at the grain boundary during base-irradiation is released during RIA because it lasts for only a few to dozens milliseconds and thus there would not be enough time for the fission gas in the matrix to diffuse to the grain boundary and then be released to the pellet-cladding gap. Therefore it is very likely to deduce that, if the fission gas release during base-irradiation is high, the RIA FGR would be low due to decreased amount of gas available for release during RIA. However, contrary to our expectation, the tests performed with fuels having higher FGR during base-irradiation, FK-series tests [14] and part of TS-series tests [15], showed high gas release during RIA. This is probably because some amount of fission gas remained in the grain boundary after base-irradiation might have been released during RIA through the inter-connected gas release network formed during base-irradiation. As for the grain size, if other conditions are the same, the smaller the grain size, the larger the inventory of fission gas at the grain boundary that would be available for release during RIA.

4. Analysis of RIA FGR data

4.1. Effect of pellet average burnup on RIA FGR

FGR under RIA conditions generally increases with pellet average burnup. This is because the higher the pellet average burnup, the larger the pellet area including HBS region from which fission gas would be released by grain boundary separation and pellet segmentation [23]. This is based on the fact that fracture strength of fuel decreases as porosity increases, and an increase of porosity in UO_2 from 5% to 20% can cause 80% reduction in fracture strength [24]. So it is possible to obtain grain boundary cracking at low temperature in the HBS region having high porosity up to around 25% [25].

The HBS width in a fuel pellet is usually considered proportional to the difference between its average burnup and the threshold one above which HBS begins to be formed [2,26]. For the case that pellet average burnup is lower than that for HBS formation, 30–40 MW d/kg U [2], it can still be assumed that release fraction would roughly be correlated with the gas amount trapped in bubbles at the grain boundaries of the pellet periphery that have retained the original microstructure. This is because, irrespective of the HBS formation, fission gas inventory at the grain boundaries in the pellet outer region remains unchanged.

Table 1
RIA test conditions and fission gas release during RIA [3,11–22].

	RIA test reactor	RIA test name	Fuel rod type	Coolant temperature at test (°C)	Grain size (μm)[a]	Pellet average burnup (MW d/kg U)	Pulse width (ms)	Energy deposition (cal/g)	Peak fuel enthalpy (cal/g)	FGR during base-irradiation (%)	FGR during RIA(%)	FGR (Base + RIA) (%)
1	CABRI	REP-Na2	PWR 17 × 17	280	_	33	9.5	207	199	0	5.5	5.5
2	CABRI	REP-Na3	PWR 17 × 17	280	_	54	9.5	122	124	0	13.7	13.7
3	CABRI	REP-Na4	PWR 17 × 17	280	_	82	76.0	95	85	0	8.3	8.3
4	CABRI	REP-Na5	PWR 17 × 17	280	_	84	8.8	104	108	0	15.1	15.1
5	CABRI	REP-Na11	PWR 17 × 17	280	_	88	31.0	104	92	0	6.8	6.8
G	NSRR	MH-1	PWR 14 × 14	20	_	39	6.8	63	47	0.2	3.5	3.7
7	NSRR	MH-2	PWR 14 × 14	20	–	39	5.5	72	54	0.2	4.2	4.4
8	NSRR	MH-3	PWR 14 × 14	20	–	39	4.5	87	67	0.2	4.0	4.2
9	NSRR	GK-1	PWR 14 × 14	20	–	42	4.6	121	93	0.4	12.8	13.2
10	NSRR	GK-2	PWR 14 × 14	20	_	42	4.6	117	90	0.4	7.0	7.4
11	NSRR	HBO-2	PWR 17 × 17	20	_	58	6.9	51	37	0	17.7	17.7
12	NSRR	HBO-3	PWR 17 × 17	20	8	58	4.4	95	74	0	22.7	22.7
13	NSRR	HBO-4	PWR 17 × 17	20	8	58	5.4	67	58	0	21.1	21.1
14	NSRR	HBO-6	PWR 17 × 17	20	8	49	4.4	109	85	0	10.4	10.4
15	NSRR	HBO-7	PWR 17 × 17	20	8	49	4.4	112	88	0	8.5	8.5
16	NSRR	TK-1	PWR 17 × 17	20	_	38	4.4	161	126	0	20.0	28.0
17	NSRR	TK-3	PWR 17 × 17	20	_	58	4.4	126	99	0	10.9	18.9
18	NSRR	TK-4	PWR 17 × 17	20	–	58	4.4	125	98	0	0.3	8.3
19	NSRR	TK-5	PWR 17 × 17	20	–	48	4.4	130	101	0	11.1	11.1
28	NSRR	TK-6	PWR 17 × 17	20	–	38	4.4	160	125	0	16.2	16.2
21	NSRR	TK-8	PWR 17 × 17	20	–	58	7.0	84	65	0	8.0	8.0
22	NSRR	OI-2	PWR 17 × 17	20	–	39	4.4	139	108	0.2	10.2	10.4
23	NSRR	OI–10	PWR 17 × 17	20	28	88	5.6	130	104	0.6	2.6	3.2
24	NSRR	OI–11	PWR	20	_	58	4.4	201	157	0.5	13.0	13.5

(*continued on next page*)

Table 1 (*continued*)

	RIA test reactor	RIA test name	Fuel rod type	Coolant temperature at test (°C)	Grain size (μm)[a]	Pellet average burnup (MW d/kg U)	Pulse width (ms)	Energy deposition (cal/g)	Peak fuel enthalpy (cal/g)	FGR during base-irradiation (%)	FGR during RIA(%)	FGR (Base + RIA) (%)
25	NSRR	OI–12	17 × 17 PWR	20	_	81	4.4	_	143	0.4	22.4	22.8
26	NSRR	JM-3	17 × 17 PWR	20	_	28	8.5	184	132	0.2	2.1	2.3
27	NSRR	TS-2	BWR 7 × 7	20	_	26	5.3	82	66	19.7	12.0	31.7
28	NSRR	TS-3	BWR 7 × 7	20	_	26	4.8	109	88	19.7	10.0	29.7
29	NSRR	TS-4	BWR 7 × 7	20	–	26	4.6	110	89	19.7	15.0	34.7
30	NSRR	TS-5	BWR 7 × 7	20	–	26	4.4	117	98	19.7	8.3	28.0
31	NSRR	FK-1	BWR 8 × 8 BJ	20	_	45	4.4	167	138	1.5	8.2	9.7
32	NSRR	FK-2	BWR 8 × 8 BJ	20	_	45	6.6	95	78	1.5	3.1	4.6
33	NSRR	FK-3	BWR 8 × 8 BJ	20	_	41	4.4	186	145	0.3	4.7	5.0
34	NSRR	FK-4	BWR 8 × 8	20	_	56	4.4	180	148	12.5	15.7	28.2
35	NSRR	FK-5	BWR 8 × 8	20	_	56	7.3	100	78	12.5	9.6	22.1
3G	NSRR	FK-6	BWR 8 × 8	20	_	61	4.4	168	131	14.2	16.9	31.1
37	NSRR	FK-7	BWR 8 × 8	20	_	61	4.4	166	129	14.2	17.0	31.2
38	NSRR	FK-8	BWR 8 × 8	20	_	61	7.3	90	65	12.8	11.3	23.3
39	NSRR	FK-9	BWR 8 × 8	20	–	61	5.7	119	98	12.8	16.6	28.6
40	NSRR	MR-1	PWR 17 × 17	20	48	71	4.0	105	89	0	8.7	8.7
41	NSRR	RH-1	PWR 17 × 17	20	–	67	4.0	122	122	0	21.4	21.4
42	NSRR	RH-2	PWR 17 × 17	280	–	67	4.0	115	99	0	26.0	26.0

[a] When grain size is unavailable, it is assumed to be 10 μm which is typical for LWR fuel.

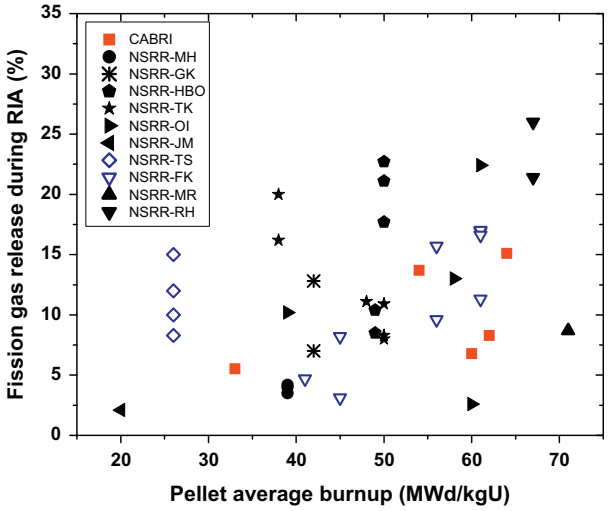

Fig. 1. RIA FGR obtained in the CABRI and NSRR tests versus pellet average burnup.

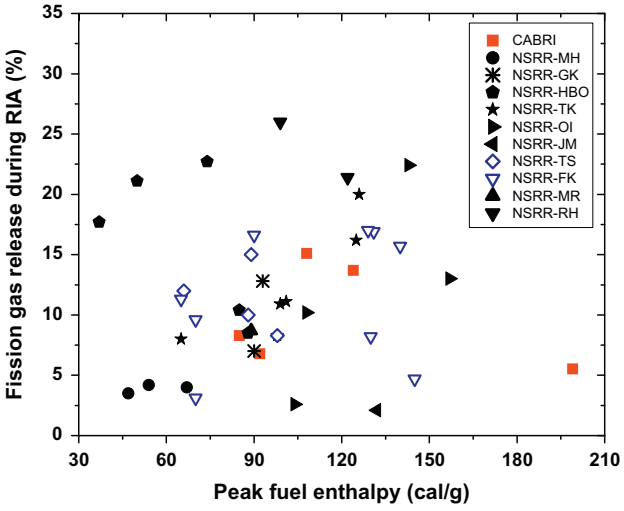

Fig. 2. RIA FGR obtained in the CABRI and NSRR tests versus peak fuel enthalpy.

Based on the argument above, it is expected that RIA FGR would increase with pellet average burnup. However, Fig. 1 shows the wide scattering even for the data with same burnup, indicating that other conditions besides burnup are dominant. In the case of the NSRR TS- and HBO-series tests [15,18] in which RIA tests were performed for fuel rods with identical burnup, FGRs are different because of the different peak fuel enthalpies. As for the NSRR FK-series tests [14], it seems that, although not so clear, RIA FGR is proportional to pellet burnup. However, it would be more appropriate to conclude that there is no direct relationship between RIA FGR and pellet average burnup or that pellet average burnup is only one of many important factors affecting RIA FGR.

4.2. Effect of peak fuel enthalpy on RIA FGR

It has been suggested that, while temperature threshold for fragmentation in the HBS region is estimated to be 1300–1500 K, grain boundary cracking takes place at about 900–1000 K [24,27]. It is certain therefore that, except for a few cases of Table 1 with low peak fuel enthalpy, fuel temperatures would have exceeded those for both pellet fragmentation and grain boundary cracking. Since fuel temperature rise in the pellet periphery during RIA can be assumed to be proportional to the peak fuel enthalpy due to nearly adiabatic heating, it is a general consensus that the degree of fragmentation and cracking of fuel and hence gas release would probably increase with peak fuel enthalpy. However, we can see no clear relationship in Fig. 2 between gas release and peak fuel enthalpy. On the contrary, we can find many cases that lower peak enthalpy produces higher gas release. For example, 3 HBO tests with peak enthalpies less than 75 cal/g yield very high FGRs of around 18–23% [18]. The opposite extreme is the CABRI REP-Na2 test [11] in which gas release was only 5.5% for a very high peak fuel enthalpy of 199 cal/g.

The fact that there is no clear relationship between RIA FGR and peak enthalpy suggests that peak enthalpy is only one of the several parameters influencing fission gas release during a RIA transient. So in the case that peak fuel enthalpy only is different with all other conditions related to fuel pellet and RIA test conditions being the same, the effect of peak fuel enthalpy on the FGR during RIA event would be clearly revealed.

4.3. Effect of the ratio of peak fuel enthalpy to pulse width on RIA FGR

A ratio of peak fuel enthalpy to pulse width, an indicator representing how fast peak fuel enthalpy is stored per unit time, can also be used to analyze the fuel behavior during a RIA event; the higher the ratio, the more gas would be released. For example, even if the peak fuel enthalpy would be the same for two RIA tests, a test with shorter pulse width would yield higher gas release due to more extensive grain boundary separation and pellet fragmentation caused by faster temperature rise. This parameter could be better than peak fuel enthalpy or pulse width in that it considers the effect of the two important parameters simultaneously.

Fig. 3 shows how the ratio of peak fuel enthalpy to pulse width affects RIA FGR. As in the case of pellet average burnup and peak fuel enthalpy, the relationship between RIA FGR and the ratio is not revealed clearly. This also implies that the effect of other parameters should be considered simultaneously to understand the gas release during a RIA event.

4.4. Effect of FGR during base-irradiation on RIA FGR

In FGR modeling, it is generally assumed that grain face is first saturated with gas bubbles and then additional gas atoms arriving after saturation migrate to the grain boundary (grain edge and grain corner) to form the release path along which gas release

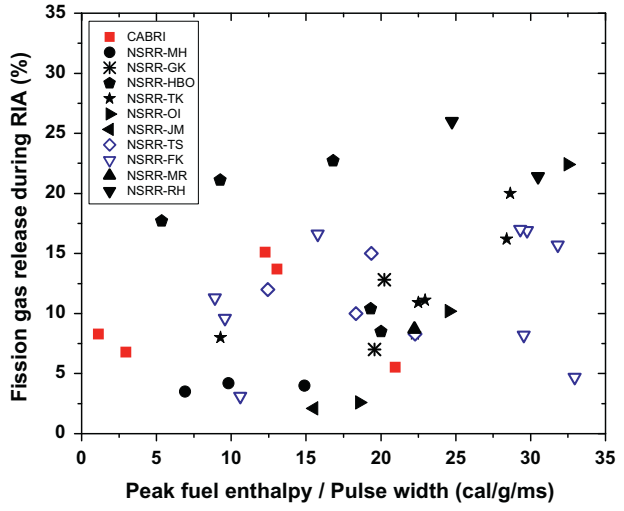

Fig. 3. RIA FGR obtained in the CABRI and NSRR tests versus the ratio of peak fuel enthalpy to pulse width.

can occur. Furthermore, the amount of gas released during base-irradiation is considered to be proportional to the degree of formation of release path [28]. Then the maximum amount of gas available for release during RIA would be the sum of fission gas at the grain face and that retained at the grain boundary. In other words, since RIA lasts for very short time of a few to dozens milliseconds, only fission gas accumulated at the grain face and grain boundary during base-irradiation would be available for release under RIA conditions, implying that there could be a proportional relationship between RIA FGR and gas release during base-irradiation. That is, the higher the base FGR, the higher the degree of release path formation along the grain boundary during base-irradiation, resulting in higher release during RIA. This argument was partly supported by the FK-series RIA tests with BWR fuel rods [14,21].

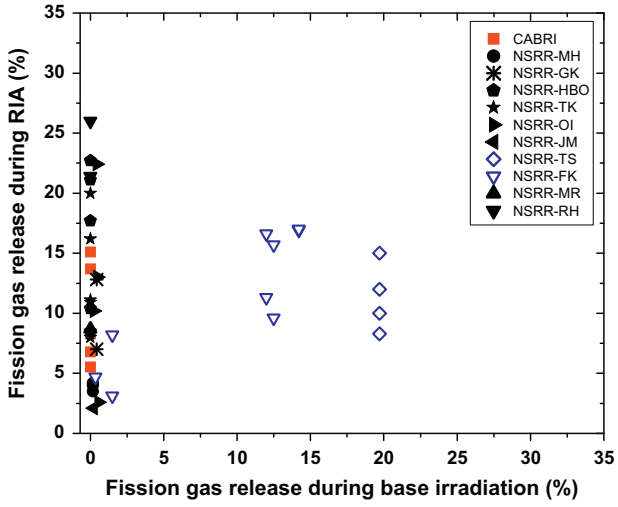

Fig. 4. RIA FGR obtained in the CABRI and NSRR tests versus during base-irradiation.

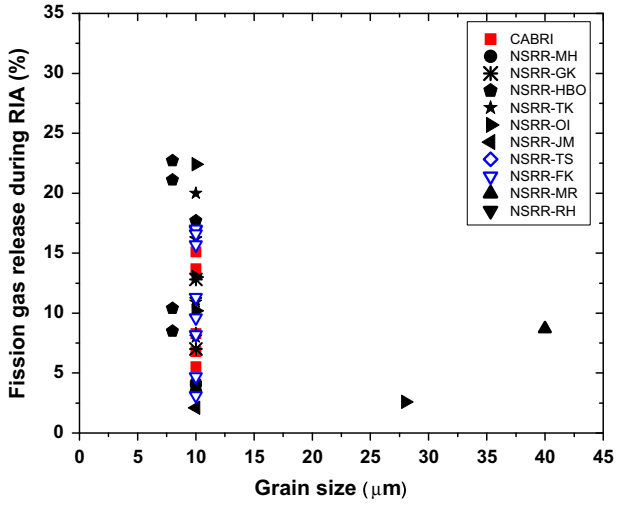

Fig. 5. RIA FGR obtained in the CABRI and NSRR tests versus grain size.

As noted in Section 2, when FGR during base-irradiation was unavailable, it was assumed to be zero. Although the FGR would have probably been greater than zero, it was difficult to estimate this quantity using information given in the open literature. Furthermore, even if we would assign some FGR values to the data points for which measured values were not present, it is very likely that the estimated value would be different from the real one, because, as it is usually observed in the database for FGR during base-irradiation, large scattering of FGR exists even for the same burnup depending on fabrication characteristics and irradiation history of fuel rod. In addition, as shown in Fig. 7, the effect of FGR during base-irradiation on RIA FGR is rather small compared to those of the other four parameters: difference in 10% for FGR during base-irradiation produces only 2.9% difference in RIA FGR. Therefore, the assumption for zero value regarding FGR during base-irradiation can be justified from the fact the effect of its value in the range of 0–10% on RIA FGR is limited.

Fig. 4 indicates that a linear relationship, which was observed in the FK-series tests [14], does not exist between RIA FGR and FGR during base-irradiation. Since it is difficult to draw any meaningful relationship in Fig. 4, we can say that other parameters should be also considered.

4.5. Effect of grain size on RIA FGR

It is known that fission gas inventory at the grain boundary and FGR are generally inversely proportional to grain size [29] with other conditions being the same. But Fig. 5 indicates that, since the grain size for most of the data is 10 μm or less, it is difficult to draw a definite conclusion on the dependence of RIA FGR on grain size.

4.6. Effect of the type of fuel rod on RIA FGR

As was discussed in Section 2, the difference between PWR and BWR fuel in terms of the pellet-cladding gap size caused by cladding creepdown could affect RIA FGR because mechanical loading on pellet would be determined by pellet cladding mechanical

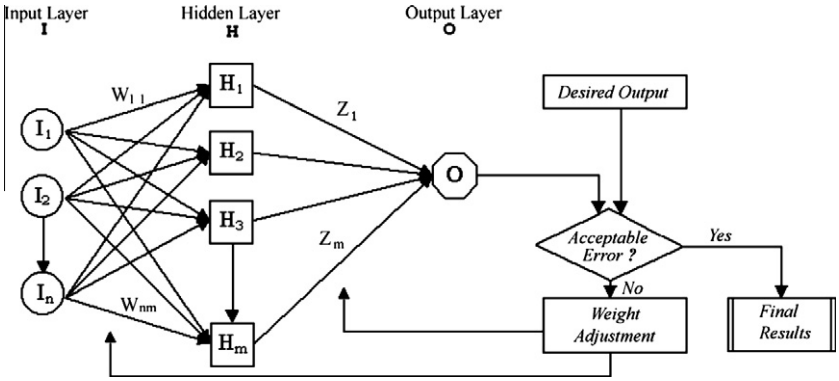

Fig. 6. Typical architecture of artificial neural network [33].

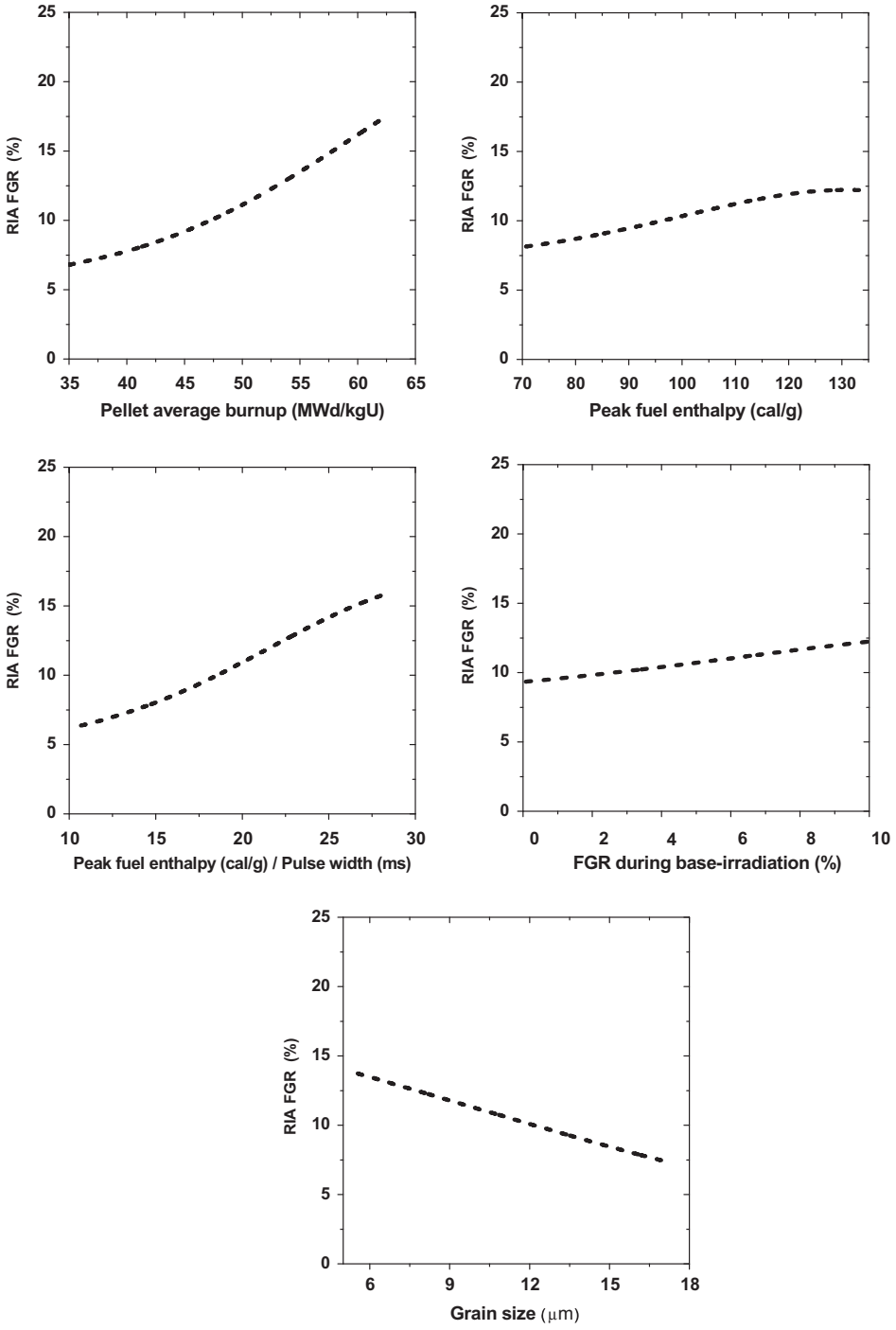

Fig. 7. Effect of the five parameters on RIA FGR predicted by the ANN model.

interaction (PCMI). In Figs. 1–5, the RIA FGR data for BWR fuels are shown as open symbols, while for PWRs as closed ones. There is no clear systematic difference between the types of fuel rods with regard to FGR under RIA conditions.

4.7. Summary of data analysis for RIA FGR

Our analysis above revealed that it was hard to explain satisfactorily the FGR during RIA using only one specific parameter. That is, irrespective of the parameters related to RIA FGR, it was difficult to find a clear pattern which can be applied to all the test data.

Therefore, rather than an analytical model based on mechanistic approach, we tried to develop an artificial neural network [8] model that can predict the RIA FGR in a typical LWR fuel rod by considering both fuel conditions before RIA and RIA test conditions itself.

5. Artificial neural network model

Artificial neural network (ANN) is a computational architecture constructed with a goal of mimicking biological networks. In more

practical terms, the ANN is a non-linear statistical data modeling tool which can be used to model complex relationships between inputs and outputs. ANN is widely used in nuclear engineering applications such as modeling of fission gas release during severe accident conditions [30], core management [31], and thermohydraulic analysis [32].

Fig. 6 shows schematically a typical architecture of ANN; input, hidden and output layer [33], and corresponding nodes (neurons). I_1 to I_n represent the input nodes, H_1 to H_m the hidden nodes, and O the output node. The factors W_{ij} and Z_k are the adjusting weights connections between input-hidden layer and hidden-output layer, respectively. Generally, the number of hidden layer is determined by trial and error seeking as few hidden layers as possible without losing accuracy of the system. One hidden layer with optimal number of nodes is generally accepted as adequate in many applications.

The nodes in the input layer correspond to independent input variables of the problem and transmit the input variables to the succeeding layer. The ANN calculates a weighted sum of input values, performs a simple mathematical operation on the sum via transfer function [34] and then passes the result onto the next layer, which is the output layer when the number of hidden layers is one, with weight factors. To implement the ANN for solving a specific problem, nodes' weights in the ANN should be properly adjusted with samples for the problem [8]. This adjusting process is called 'training'. There are many training algorithms but we used the most popular training algorithm, back propagation algorithm [34].

The back propagation algorithm requires sample training data with desired output. After presenting a training sample to the ANN, the ANN's output is compared with the desired output from that sample and then the errors in output nodes are calculated. As the algorithm's name implies, the errors propagate backwards from the output nodes to the inner ones. The back propagation is used to calculate the gradient of the error of the network with respect to the network's modifiable weights. Then, it looks for the weights that minimize the error [35].

6. ANN model for RIA FGR

An ANN model implemented in this paper consists of one input layer, two hidden layers, and one output layer. It is important to select an appropriate number of input parameters in ANN because too many input parameters will drastically slow down the learning process. In this work, of the various parameters that can be used as input, the five ones analyzed in Section 4 are chosen for five nodes on the input layer; pellet average burnup, peak enthalpy, the ratio of peak fuel enthalpy to pulse width, FGR during base-irradiation, and grain size of fuel pellet.

The first hidden layer has five nodes and the second hidden layer has two nodes, which are optimized by a comparison of the calculation results with the measured data. One output node on the output layer is used for the fission gas release during RIA tests. The hyperbolic tangent function is used for the transfer function of the ANN.

The ANN model for RIA FGR was trained and then developed using a back propagation algorithm [34] for the data set of Table 1. Usually half of the data is used for training and the other for predicting, because if all the data are used for training, it is difficult to know if the developed ANN model could be applied to predict data obtained in different conditions. In our case, however, since the number of data points 42 is rather small, we used 37 data for training. The remaining five data points (FK-3, GK-1, HBO-2, HBO-3, and HBO-4) were excluded because their deviation from the general trend misled the training of the ANN model.

7. Results and discussion

7.1. Sensitivity study of the ANN model

Using the developed ANN model, the effect of each input parameter on RIA FGR was studied to see if the model would give physically reasonable results. Fig. 7 shows how the RIA FGR depends on each parameter with the other four ones being fixed at their respective means calculated from the data set of Table 1. While RIA FGR increases with the pellet average burnup, peak fuel enthalpy, the ratio of peak fuel enthalpy to pulse width, and FGR during base-irradiation, larger grain gives smaller RIA FGR. Therefore, it can be concluded that the present ANN model provides a physically acceptable result.

Fig. 8 shows the sensitivity analysis results of the ANN model, providing a measure of the relative importance of each parameter for RIA FGR. For example, the sensitivity of 3.2% for pellet average burnup is calculated as follows. First, the mean and standard deviation value of the pellet average burnup are derived from the 42 data points of Table 1, where the mean and one standard deviation are 48.5 and 13.5 MW d/kg U, respectively. Then, with the other four input parameters being fixed at their respective mean values obtained also from the data, the RIA FGRs are calculated for the pellet average burnups which are evenly divided into 100 intervals between one standard deviation lower than the mean (35 MW d/kg U) and one standard deviation higher than the mean (62 MW d/kg U). Finally, from the 100 calculations of RIA FGR made by the ANN model, the sensitivity defined as one standard deviation of the calculated FGRs is obtained. The sensitivities for the other parameters are obtained by the same procedure. Fig. 8 indicates that, although the pellet average burnup and the ratio of peak fuel enthalpy to pulse width are two of the most important parameters, the other three also play a comparable role, suggesting that the five parameters were chosen well.

7.2. Analysis of the test data by the ANN model

Fig. 9a compares the calculated RIA FGR by the ANN model with the measured data. Except for the seven data points whose test names are shown in the figure, the ANN model predicts FGR within the uncertainty of ±4% for the remaining 35 cases, which corresponds to 83% of the total data.

An investigation was made to explain why in contrast with other cases a rather big discrepancy exists for the seven tests; in other words, why they show unusual behavior from the viewpoint of RIA FGR. As for the three HBO-series tests (HBO-2, -3 and -4) that experienced very high fission gas release (17.7–22.7%) for low peak fuel enthalpies (37–74 cal/g) [18], PIE showed that these

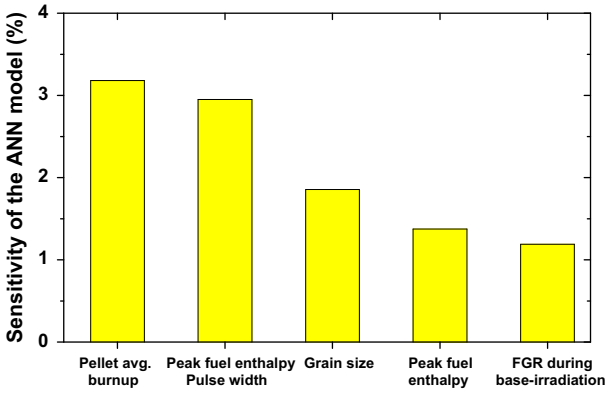

Fig. 8. Sensitivity of the ANN model for the five parameters.

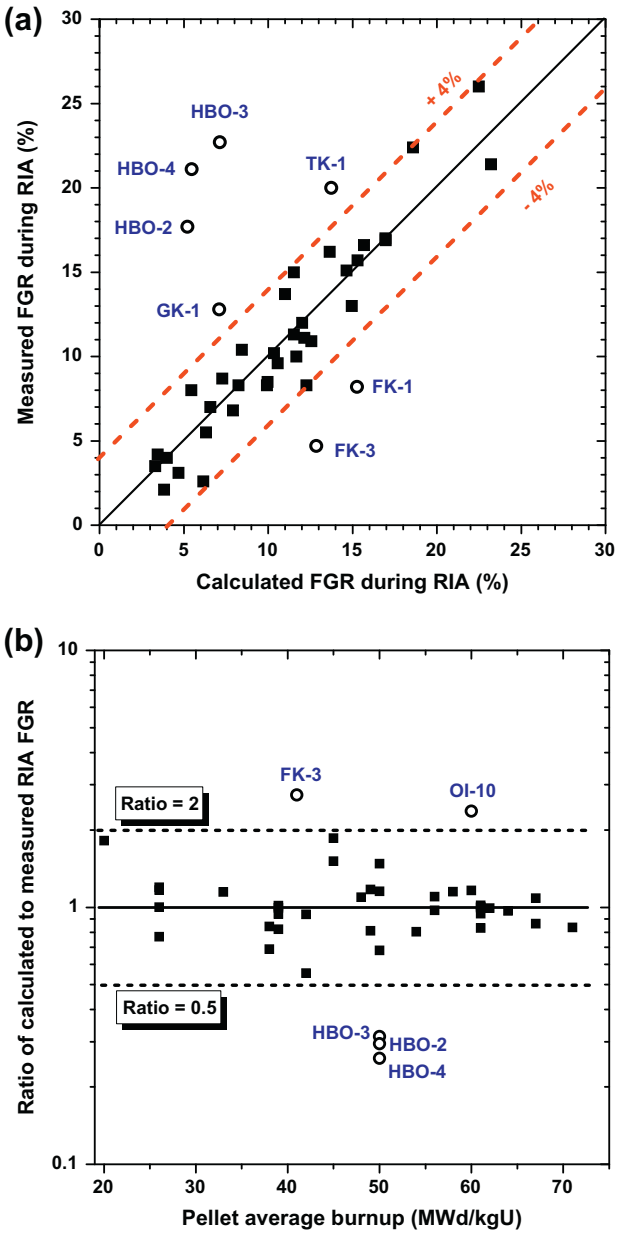

Fig. 9. (a) Comparison of RIA FGR calculated by the ANN model with measured value and (b) ratio of calculated to measured RIA FGR versus pellet average burnup.

fuels had fine microcracks in the pellet periphery that were much more significant than others undergoing similar RIA test conditions [19]. However, the reason for the formation of the unusually high number of microcracks was not clearly revealed.

As for FK-1 and FK-3 [14], they showed rather low FGR of 8.2% and 4.7% for the relatively high peak fuel enthalpies of 130 and 145 cal/g, respectively. This might be linked to the low FGR (1.5% and 0.3%) during base-irradiation, because this implies that, at the outer part of fuel pellet where most of the retained gas could be released during RIA, either the release path was not effectively formed or the amount available for release at the grain boundaries was low. In support of this argument, detailed examination of FK-1 provided the evidence that most fission gas was released from the center region of the test fuel pellet during RIA test [36].

GK-1 with burnup of 42 MW d/kg U had a rather high FGR of 12.8% for a moderate peak enthalpy of 93 cal/g. PIE after the test showed that it had several microcracks at the pellet periphery that were considered to be generated by a very steep temperature gradient produced during the very quick heating in the pulse irradiation [20].

The RIA FGR of TK-1 (20%), corresponding to all the fission gas accumulated in the grain boundaries [14], is very high considering its burnup (38 MW d/kg U) – low for the formation of high burnup structure – and the peak fuel enthalpy of 126 cal/g that would have led to the peak centerline temperature far below than a threshold one (2100 K) for intragranular gas migration by diffusion in the pellet central region [3]. Ceramography showed extensive pellet cracking in the fuel pellet of TK-1 [36]. From all this information, it is deduced that, even if the HBS is not formed or HBS width is very limited in the pellet periphery, fission gas can be released by the separation of as-manufactured grains in the outer part of fuel pellet during RIA.

Fig. 9b shows the ratio of calculated to measured RIA FGR as a function of pellet average burnup. Three data points of HBO-series test (HBO-2, -3, and -4) have ratios lower than 0.5, and FK-3 and OI-10 have ratios higher than 2. The reason for a large deviation of the three tests of HBO-series and FK-3 from the calculations was explained above. As for OI-10, while a large grain size of 28 μm [16] yielded a lower FGR (2.6%), the calculated value was high due to the relatively high burnup (60 MW d/kg U) and high peak fuel enthalpy (104 cal/g).

Table 2 summarizes the reason why there exists a big difference between the measured and calculated RIA FGRs for seven cases (HBO-2, HBO-3, HBO-4, TK-1, GK-1, FK-1 and FK-3).

7.3. Application of the ANN model to LWR fuel

The present ANN model was applied to LWR fuel rods to estimate how much gas would be released under typical RIA conditions. Input values of the five parameters for LWR fuel were chosen as shown in Table 3. The grain size of fuel pellet is assumed to be 10 μm since this is a typical value for LWR fuel. The pulse width for rod drop accident in BWRs is estimated to be 100 ms [37], and the one for rod ejection accident in PWR is in the range of 25–40 ms [38]. Therefore, to cover the pulse width for both PWR and BWR fuel, three values of pulse widths—20, 60 and 100 ms—were chosen for parametric analysis. The maximum fuel enthalpy change in PWR is given as 100 cal/g [37]. In most cases, FGR during base-irradiation does not exceed 10% and so the upper limit is taken to be 10%. To cover the fuel burnup reached in recent LWR fuel, the maximum pellet burnup is given as 80 MW d/kg U. And the minimum burnup of 20 MW d/kg U is selected because it is the lowest burnup in the database (see Table 1) used for this analysis.

By combining the respective values for the five parameters, a total of 180 calculations (36 for each of the five burnups 20, 35, 50,

Table 2
Reason for the differences between the measured and calculated RIA FGRs.

Test	Unexpected results	PIE observation
HBO-2, HBO-3, HBO-4	High FGR (17.7–22.7%) for low peak fuel enthalpies (37–74 cal/g)	Much more fine cracks in the pellet periphery than other fuels [19]
TK-1	High FGR (20%) for medium burnup (38 MW d/kg U)	Extensive pellet cracking in the fuel pellet led to large gas release [36]
GK-1	High FGR (12.8%) for 42 MW d/kg U and 93 cal/g	A certain number of microcracks at the pellet periphery [20]
FK-1, FK-3	Low FGR for high peak fuel enthalpy: FK-1 (8.2%/130 cal/g), FK-3 (4.7%/145 cal/g)	Release path was not formed in the pellet periphery during base-irradiation [36]

Table 3
Parameters for the application of the ANN model to typical LWR RIA conditions.

Parameters	Values
Grain size (m)	10
Pulse width (ms)	20, 60, 100
Peak fuel enthalpy (cal/g)	40, 60, 80, 100
FGR during base-irradiation (%)	0, 5, 10
Pellet average burnup (MW d/kg U)	20, 35, 50, 65, 80

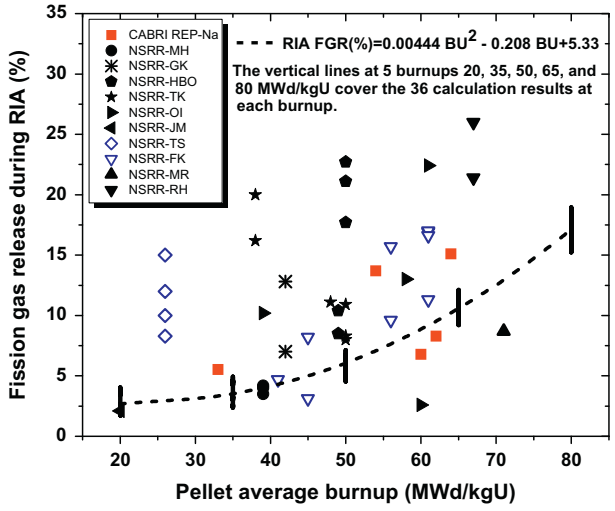

Fig. 10. Comparison of the ANN model's calculation for typical RIA conditions of LWR fuel with the measured data obtained in the CABRI and NSRR tests.

65, and 80 MW d/kg U) were made by the present ANN model to calculate RIA FGR. The median FGRs for the 36 calculations at the five burnups, 2.9–17.1%, can be fitted by a quadratic formula as shown in Fig. 10: RIA FGR (%) = 0.00444 BU^2 – 0.208 BU + 5.33, where BU is a pellet average burnup (MW d/kg U). The vertical lines at the five burnups, whose magnitudes are 1.2–1.9%, show the spread of the 36 calculations at each burnup. When considering these spreads depending on the combination of the input values for the parameters, RIA FGR is calculated to be 1.7–14.0% for the pellet average burnup ranging from 20 to 70 MW d/kg U—the minimum and maximum burnup for the database of this work.

The quadratic formula in Fig. 10 is derived as follows. First, for each of five pellet average burnups, 36 RIA FGRs are calculated by the ANN model. Then the median FGR of the 36 results is assumed to be the representative value for the burnup being considered. Since five representative FGRs are available for five pellet average burnups, we can derive a formula which can fit them best. In contrast to general observation that RIA FGR would be proportional to burnup, this study suggests that burnup has a stronger influence on RIA FGR than expected; in other words, RIA FGR increases with the square of burnup.

The reason why RIA FGR for LWR conditions is expressed in terms of pellet average burnup is that the other four parameters would be either fixed more or less or determined to a certain degree in LWR. Grain size of fuel pellet is around 10 μm in most cases. Pulse width and peak fuel enthalpy – consequently the ratio of peak fuel enthalpy to pulse width – would deviate only slightly from their typical values in both PWR or BWR. And the effect of FGR during base-irradiation in the range of 0–10% is limited as shown in Fig. 10. Therefore, pellet average burnup only would be a dominant parameter affecting RIA FGR under typical LWR conditions.

The key difference between the two predictions for Figs. 9 and 10 is that, although the same ANN model was used, different input parameters—especially pulse width—were used for the two cases: shorter one for CABRI and NSRR test (less than 10 ms except for just two cases of REP-Na4 and REP-Na11 with pulse widths of 76 and 31 ms, respectively,) and longer one for the calculations for the fitting line of Fig. 10 (20–100 ms). As expected, Fig. 10 shows that, in most cases, RIA FGRs under LWR conditions are lower than those obtained in CABRI and NSRR tests at the same burnup mainly due to the effect of longer pulse width. This implies that the ANN model provides a reasonable result and accordingly the model developed in this work can be applied to predict RIA FGR in LWR fuel.

8. Conclusions

Since the fission gas release during RIA is important in determining mechanical load on fuel cladding, RIA FGR obtained in CABRI and NSRR tests were analyzed in terms of five parameters: pellet average burnup, peak fuel enthalpy, the ratio of peak fuel enthalpy to pulse width, fission gas release during base-irradiation, and grain size. The analysis revealed that, to understand the release behavior during RIA, all the relevant parameters affecting fuel behavior should be considered simultaneously.

A fission gas release model based on ANN method was developed using the CABRI and NSRR data. The model predicts the fission gas release under RIA conditions as a function of the five parameters mentioned above. Parametric study of the model shows a physically reasonable trend for the five parameters. And it also reveals that, although the pellet average burnup and the ratio of peak fuel enthalpy to pulse width are two of the most important parameters, the other three also play a comparable role, suggesting that the five parameters were chosen well. The model was applied to calculate FGR during RIA events of typical LWRs, yielding 1.7–14.0% depending on the combination of inputs for the five parameters.

Regarding radioactive source term under RIA conditions, the ANN model of this work is only able to consider the case that fuel rod remains intact during RIA; the model predicts the fission gas inventory in the pellet-cladding gap available for release when fuel cladding fails. On the other hand, for the case that fuel failure occurs at high enthalpy under a RIA event, the source term should be analyzed using test results obtained at high enthalpies leading up to fuel fragmentation or melting [39].

Acknowledgments

The Ministry of Education, Science and Technology (MEST) of the Republic of Korea has sponsored this work through the Mid- and Long-term Nuclear R&D Project.

References

[1] F. Schmitz, J. Papin, J. Nucl. Mater. 270 (1999) 55.
[2] Yang-Hyun Koo, Byung-Ho Lee, Oh Jae-Yong, Kun-Woo Song, Nucl. Technol. 164 (2008) 337.
[3] J. Papin, M. Balourdet, F. Lemoine, F. Lamare, J.M. Frizonnet, F. Schmitz, Nucl. Safety 37 (1996) 289.
[4] W. Liu, A. Romano, M. Kazimi, Modeling high burnup fuel fission gas release and swelling during fast transients, in: International Topical Meeting on LWR Fuel Performance, Orlando, Florida, September 19–22, 2004.
[5] W. Liu, M. Kazimi, Modeling high-burnup BWR fuel behavior, in: International Conference on LWR Fuel Performance, Kyoto, Japan, October 2–6, 2005.
[6] J.C. Latche, F. Lamare, M. Cranga, Computing reactivity initiated accidents in PWRs, SMIRT-13 Meeting, Porto Alegre, Brazil, August 13–18, 1995.
[7] E. Federici, F. Lamare, V. Bessiron, J. Papin, Status of development of the SCANAIR code for the description of fuel behavior under reactivity initiated accident, in: International Topical Meeting on LWR Fuel Performance, Park City, Utah, April 10–13, 2000.

[8] NeuroSolutions 5 Manual, NeuroDimension, Inc., 2009. <www.nd.com>
[9] L. Jernkvist, A. Massih, P. Rudling, A Strain-based Clad Failure Criterion for Reactivity Initiated Accidents in Light Water Reactors, TR 03-008, Quantum Technologies AB, Uppsala, Sweden, 2003.
[10] P. MacDonald, S. Seiffert, S. Matindon, Z. Martinson, R. MaCardell, D. Owen, S. Fukuda, Nucl. Safety 21 (1980) 582.
[11] J. Papin, B. Cazalis, J.M. Frizonnet, J. Desquines, F. Lemoine, V. Georgenthum, F. Lamare, M. Petit, Nucl. Technol. 230 (2007) 157.
[12] T. Fuketa, H. Sasajima, T. Sugiyama, Nucl. Technol. 133 (2001) 50.
[13] T. Sugiyama, Y. Udagawa, M. Umeda, T. Fuketa, PWR fuel behavior in RIA-simulating experiment at high temperature, in: Water Reactor Fuel Performance Meeting, Seoul, Korea, October 19–23, 2008.
[14] T. Fuketa, F. Nagase, T. Nakamura, H. Uetsuka, K. Ishijima, NSRR pulse irradiation experiments and tube burst tests, in: Proc. 28th Water Reactor Safety Information Mtg., Bethesda, Maryland, October 23–25, 2000 (NUREG/CP-0172/XAB, US NRC (2000)).
[15] T. Nakamura, M. Yoshinaga, M. Sobajima, K. Ishijima, T. Fujishiro, Nucl. Technol. 108 (1994) 45.
[16] T. Fuketa, T. Sugiyama, F. Nagase, J. Nucl. Sci. Technol. 43 (2006) 1080.
[17] T. Fuketa, T. Sugiyama, M. Umeda, K. Tomiyasu, H. Sasajima, Behavior of high burnup PWR fuels during simulated reactivity-initiated accident conditions, in: International Meeting on LWR Fuel Performance, Salamanca, Spain, October 22–26, 2006.
[18] T. Fuketa, F. Nagase. K. Ishijima, T. Fujishiro, NSRR/RIA experiments with high burnup PWR fuels, in: ANS LWR Fuel Performance Meeting, Portland, Oregon, March 2–6, 1997.
[19] T. Fuketa, Y. Mori, H. Sasajima, K. Ishijima, T. Fujishiro, Behavior of high burnup PWR fuel under a simulated RIA condition in the NSRR, in: Proc. CSNI Specialists Mtg. on Transient Behavior of High Burnup Fuel, Cadarache, France, September 12–14, 1995 (NEA/CSNI/R(95)22, Nuclear Energy Agency (1996)).
[20] T. Fujishiro, K. Yanagisawa, K. Ishijima, K. Shiba, J. Nucl. Mater. 188 (1992) 161.
[21] T. Nakamura, K. Kusagaya, T. Fuketa, H. Uetsuka, Nucl. Technol. 138 (2002) 253.
[22] T. Fuketa, T. Sugiyama, F. Nagase, M. Suzuki, JAEA studies on high burnup fuel behaviors during RIA and LOCA, in: International Topical Meeting on LWR Fuel Performance, San Francisco, California, September 3–October 3, 2007.
[23] F. Lemoine, J. Nucl. Mater. 248 (1997) 238.
[24] F. Lemoine, F. Schmitz, Impact of fission gas on irradiated PWR fuel behavior at extended burnup under RIA conditions, in: Proc. CSNI Specialists Mtg. Transient Behavior of High Burnup Fuel, Cadarache, France, September 12–14, 1995, NEA/CSNI/R(95)22, p. 493, Nuclear Energy Agency (1996).
[25] W. Goll, Ch. Hellwig, P.B. Hoffmann, W. Sauser, J. Spino, C.T. Walker, Int. J. Nucl. Power 52 (2007) 95.
[26] Yang-Hyun Koo, Byung-Ho Lee, Jin-Sik Cheon, Dong-Seong Sohn, J. Nucl. Mater. 295 (2001) 213.
[27] S.R. Pati, A.M. Garde. L.J. Clink, Contribution of pellet rim porosity to low temperature fission gas release at extended burnups, in: Proceeding of the International Topical Meeting in Light Water Reactor Fuel Performance, Williamsburg, Virginia, April 17–20, 1988.
[28] Yang-Hyun Koo, Byung-Ho Lee, Dong-Seong Sohn, J. Nucl. Mater. 280 (2000) 86.
[29] D.R. Olander, Fundamental Aspects of Nuclear Reactor Fuel Elements, TID-26,711–P1, Technical Information Center, Energy Research and Development Administration, Oak Ridge, TN, 1976.
[30] W.S. Andrews, B.J. Lewis, D.S. Cox, J. Nucl. Mater. 270 (1999) 74.
[31] H.G. Kim, S.H. Chang, B.H. Lee, Nucl. Sci. Eng. 113 (1993) 70.
[32] A. Ridluan, M. Manic, A. Tokuhiro, Nucl. Eng. Des. 239 (2009) 308.
[33] H. Mazrou, Nucl. Eng. Des. 239 (2009) 1901.
[34] H. Demuth, M. Beale, Neural Network Toolbox for use with MATLAB. User's Guide Version 6.5, The MathWorks Inc., Natick, MA, 2002.
[35] http://en.wikipedia.org/wiki/Backpropagation.
[36] M. Amaya, T. Sugiyama, T. Fuketa, J. Nucl. Sci. Technol. 41 (2004) 966.
[37] R.O. Meyer, Nucl. Technol. 155 (2006) 293.
[38] H. Ferroukhi, M. Zimmermann, Ann. Nucl. Energy 36 (2009) 1170.
[39] B.J. Lewis, F.C. Iglesias, R.S. Dickson, A. Williams, J. Nucl. Mater. 394 (2009) 67.